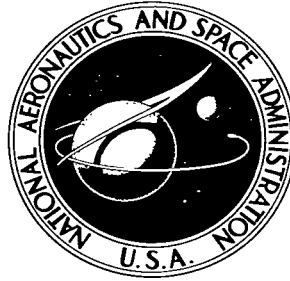


NASA TECHNICAL NOTE



NASA TN D-3407

NASA TN D-3407

LOAN COPY: F
AFWL (V
KIRTLAND AI



THRUST MEASUREMENT OF SERT I ION THRUSTORS

by William C. Nieberding and Robert R. Lovell

Lewis Research Center

Cleveland, Ohio





THRUST MEASUREMENT OF SERT I ION THRUSTORS

By William C. Nieberding and Robert R. Lovell

Lewis Research Center
Cleveland, Ohio

NATIONAL AERONAUTICS AND SPACE ADMINISTRATION

For sale by the Clearinghouse for Federal Scientific and Technical Information
Springfield, Virginia 22151 - Price \$2.00

THRUST MEASUREMENT OF SERT I ION THRUSTORS

by William C. Nieberding and Robert R. Lovell

Lewis Research Center

SUMMARY

A description and an analysis of the thrust detection systems aboard the SERT I (Space Electric Rocket Test) ion thruster flight test are given. Two types of thrust detection were employed: (1) sun sensor spacecraft spin period detectors and (2) a radial accelerometer centripetal acceleration detector. The thrust of a 22-millinewton ion thruster produced a rate of change of spacecraft spin of approximately 0.01 percent per second. This change was measured by both detection systems to yield direct thrust measurements agreeing to within 5 percent for 10- to 30-second averages. The radial accelerometer was also used as a very sensitive precession detector. The precession half-cone angle of the spacecraft was measured to be 5.3×10^{-4} radian (0.03°).

INTRODUCTION

The flight of SERT I, directed by the Lewis Research Center, on July 20, 1964, marked the first successful production of thrust by an ion thruster in space. This report discusses the instrument systems used to measure the thrust produced. Included will be a description of the systems, an analysis of their function and accuracy, and a summary of the results obtained from the data produced by them. A report of the overall results of the SERT I flight has been published (ref. 1); thus, only the features of the experiment salient to the subject at hand will be discussed.

The primary objective of the SERT I flight experiment (refs. 1 and 2) was to confirm that an ion beam could be neutralized in space. A contact-ionization thruster using cesium propellant and an electron-bombardment thruster using mercury propellant, which produced maximum expected thrusts of 7 and 25 millinewtons, respectively, were to be the first ion thrusters operated in space. In order that beam neutralization might be demonstrated most conclusively, the spacecraft was designed to permit direct measurement of thrust. The presence of thrust for an appreciable time would be impossible were neutralization lacking.

Prior to the SERT I flight some indirect measurements of ion thruster thrust had been made during vacuum-chamber testing. The method used was to place a pendulum-type target in the ion stream and detect the deflection produced by the impinging beam (ref. 3). Agreement was within 10 percent between the measured thrust values and those theoretically calculated on the basis of electrical measurements.

The spacecraft was launched into a suborbital trajectory providing approximately 1 hour of experiment time. Vacuum-chamber testing of the thrusters indicated that high-voltage breakdown would probably occur and cause the thrust to be intermittent, with bursts as short as a few seconds duration. This fact plus the low expected thrust level were the conditions which established the basic configuration of the SERT I spacecraft such that a measurement of thrust, hence beam neutralization, could be made.

The two ion thrusters were mounted so that their thrust would cause a torque about the spin axis of the spin-stabilized spacecraft, and hence, a change in spin rate. This would allow the detection of short low-level pulses of thrust by measuring the integrated effect on spin rate. Thrust was thus determined by measuring spin rate and its rate of change.

There were two spin-rate detection systems employed. The first consisted of two independent, redundant, sun sensor, spin period detectors, each of which transmitted one pulse per spacecraft revolution by way of separate telemetry links to the ground stations. The period between successive pulses from either sensor was then measured with ground based precision electronic counters. The second system consisted of an accelerometer mounted so that it sensed the centripetal acceleration due to spacecraft spin. Its output signal was transmitted redundantly through both telemetry links.

Two ground receiving stations were used to acquire the data, Wallops Island, Virginia, and Bermuda. Identical thrust measurement ground equipment was located at each station.

SYSTEM DESCRIPTIONS

Simplified Spacecraft Configuration

The basic, simplified configuration of the SERT payload was that of a right circular disk spinning about its longitudinal axis (fig. 1). While this configuration differs considerably from that of the actual payload (see figs. 2 and 3), it serves as a model adequate for the thrust detection analysis. Where deviations from this model are significant to the analysis, corrections or allowances will be made, and these will be made evident.

The two ion thrusters were mounted opposite each other on arms extending out from the disk on the x-axis (fig. 1). (Note that the axes shown in fig. 1 are fixed in the disk.)

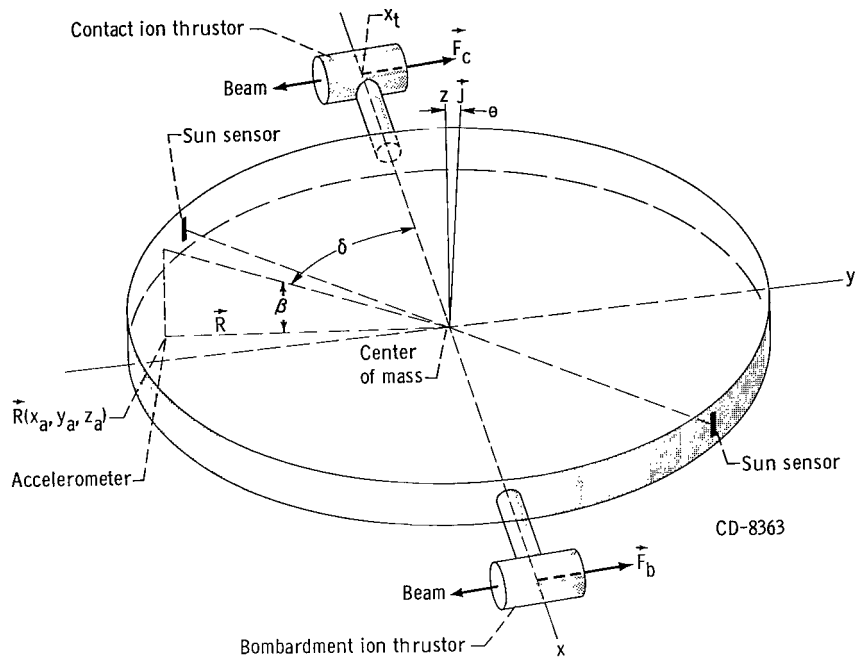


Figure 1. - Simplified payload configuration.

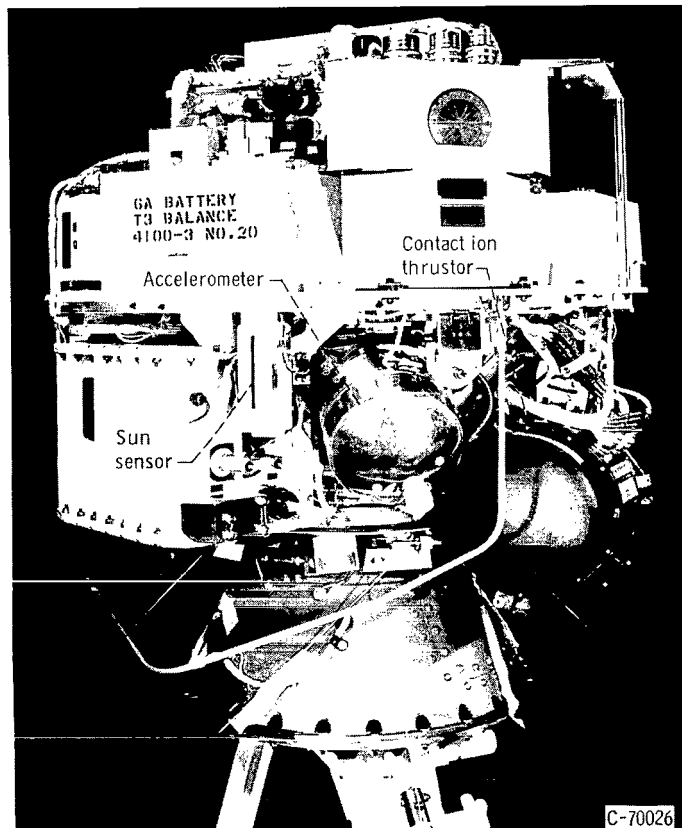


Figure 2. - SERT payload with arms folded.

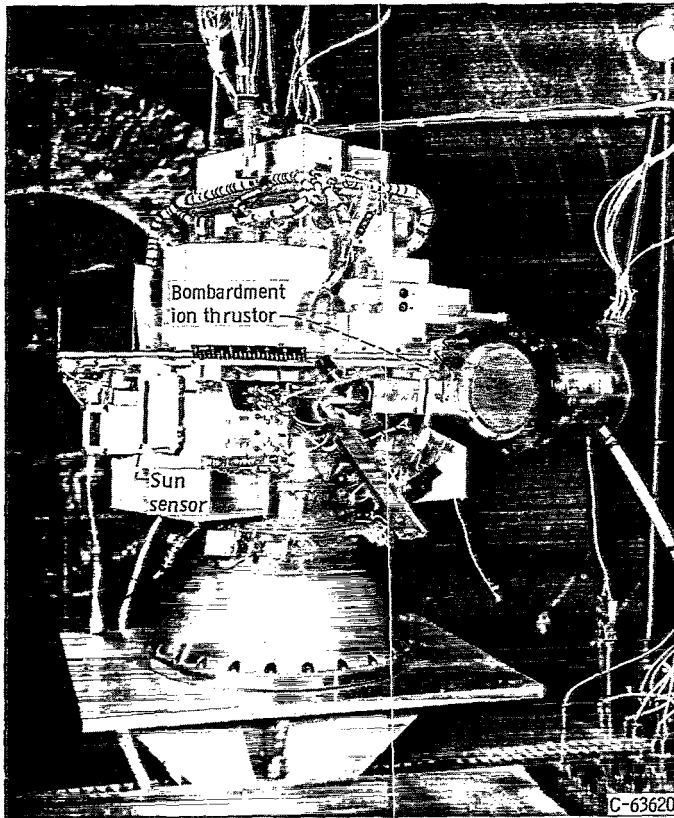


Figure 3. - SERT payload with arms extended.

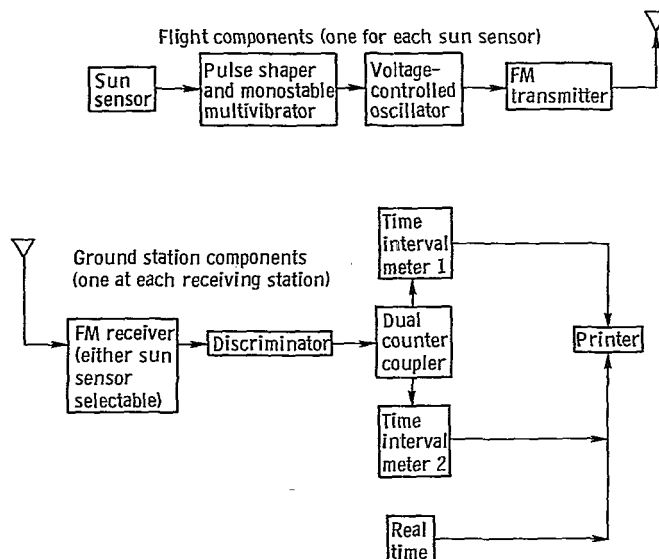


Figure 4. - Sun sensor system.

During launch the thrusters were folded down (fig. 2) under the disk to fit inside the nose cone. The significant sequence of events, as planned, was

- (1) Launch, by an NASA Scout rocket, through third-stage burnout
- (2) Nose cone ejection
- (3) Spin up of fourth stage and payload (with small solid fuel rockets)
- (4) Fourth stage burn
- (5) Fourth-stage separation from payload
- (6) Thrustor deployment
- (7) Contact ion thruster burn (approximately 20 min)
- (8) Contact ion thruster shutdown
- (9) Bombardment ion thruster burn (approximately 20 min)
- (10) Reentry

This report will be concerned primarily with the sequence after step (6). With the thrusters deployed, the payload would have a spin rate ($+\omega_z$) of about 10 radians per second, which was required for spin stability, and its z-axis would be precessing about its angular momentum vector with an instantaneous half-cone angle θ . (Symbols are defined in appendix A.) There were energy dissipating precession dampers on the payload to reduce θ to a maximum of 0.035 radian (2°). For smaller θ the dampers were inoperative.

The thrust vectors of the two ion thrusters were both parallel to the y-axis and in the +y-direction, and the

result would have been a -z-torque (i. e. , despin) from the contact ion thruster and a +z-torque (i. e. , spinup) from the bombardment ion thruster. There would be a despin followed by a spinup. The basic problem was to determine the thrust of the thrusters by measuring the very slight rate of change of ω_z .

The following sections will describe the systems used to make this measurement. First will be described the sun sensor and its associated system and then the accelerometer with its associated system.

Sun Sensor

Sun sensor system. - There were two sun sensors located approximately π radians apart on the spacecraft base plate. Each sent its signal through separate flight equipment and a separate telemetry system. At each ground receiving location either sun sensor signal could be selected, the choice resting upon signal quality. Figure 4 shows a block diagram of one of the sun sensor systems. The flight components, separate but identical for each sensor, consisted of a sun sensor, pulse shaper, subcarrier oscillator, transmitter, and antenna. The ground based equipment at each receiving station consisted of an antenna, a receiver, a discriminator, two precision electronic time-interval meters, and a printer.

The sun sensor, which produced 1 pulse per revolution of the spacecraft with respect to the sun, was mounted on the periphery of the spacecraft base plate, as shown in figures 1 to 3. As the spacecraft revolved about its spin axis, sun rays passed through the narrow vertical slit (fig. 5) in the front of the sensor housing and illuminated a photovoltaic cell mounted at the rear of the housing. The output of the photovoltaic cell was amplified and used to trigger a monostable multivibrator, which, in turn, was used to modulate a standard IRIG voltage-controlled subcarrier oscillator. This subcarrier was then one of the channels of the telemetry link.

On the ground, after reception and discrimination, the signal was a replica of the monostable multivibrator output. This pulse train was sent through a dual-counter coupler in such a way that the period between successive pulses was measured alternately with two precision time-interval meters. The output of these meters and real time were recorded on a printer.

Launch time effect on sun sensor. - To ensure illumination of the sensor by the sun and to prevent illumination by the Earth or moon, the time of launch was chosen to optimize the angle between the spacecraft spin axis and the line joining the sun and spacecraft. As the spacecraft spun about its axis of maximum moment of inertia, the geometric line of sight limits of the sun sensor swept out a triangle of revolution (fig. 5). The upper limit of the triangle of revolution was determined by the length and location of

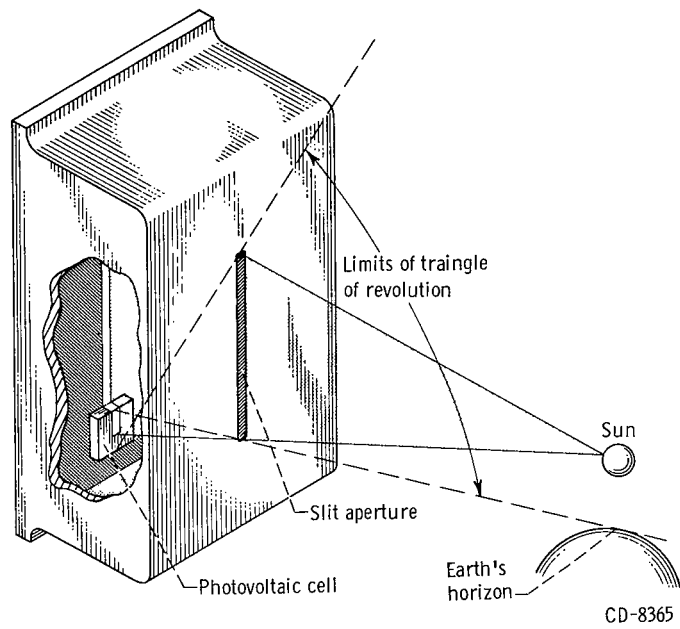


Figure 5. - Sun sensor.

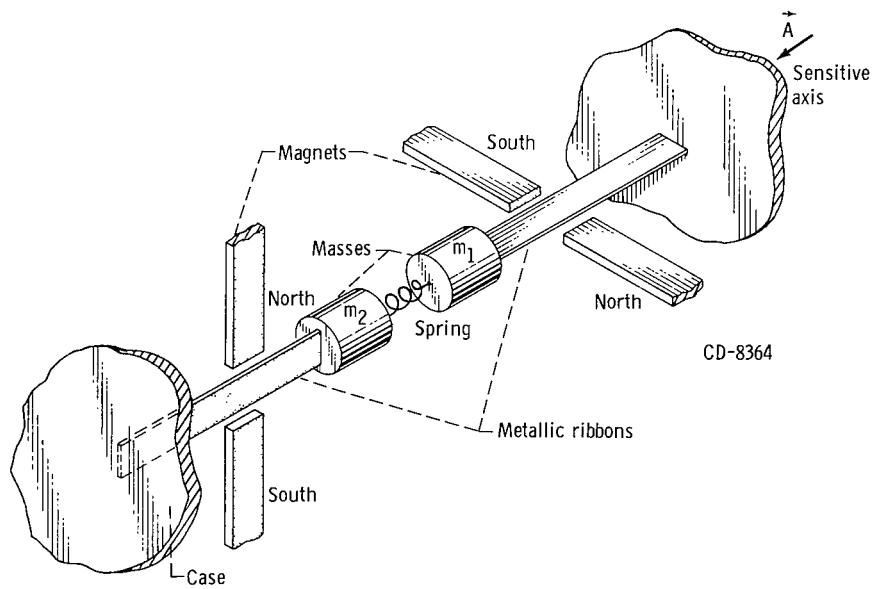


Figure 6. - Simplified accelerometer.

the slit aperture with respect to the photocell at the rear of the sun sensor housing. To minimize thrust error due to nutation and precession, the angle between the sun and spin axis should have been $\pi/2$ radians, but the trajectory and, hence, the attitude of the spacecraft with respect to the Earth was optimized for maximum experiment time. The 3σ limit on the angle between the spin axis and a line from the photocell through the slit to the Earth's horizon fixed the lower limit of the triangle of revolution at 1.5 radians (85°). The upper limit of the triangle of revolution was fixed at $\pi/3$ radians (60°) by the housing geometry. The angle between the sun and the spin axis was computed as a function of Greenwich mean time (see appendix B). The launch time was chosen to place the sun as near as possible to 1.5 radians (85°) and to place the moon outside the triangle of revolution.

Accelerometer System

Accelerometer. - The accelerometer was one of the type known as "vibrating string" instruments. A schematic view of this type of instrument, in which the strings are replaced by ribbons, is shown in figure 6.

If an acceleration \vec{a} acts along the sensitive axis \vec{A} of the instrument, then a tension force \vec{F}_S , equal to $m\vec{a}$, will be exerted on the thin metallic ribbon ($m = m_1$ or m_2). The mechanical resonant frequency of a string in tension is

$$f_r = B \sqrt{F_S + F_I}$$

where B is a constant and F_I is an initial tension supplied by the spring. Thus, the resonant frequency of the string is a function of the acceleration. If two of these string-restrained mass systems are opposed (see fig. 6), then the tension in one increases while the tension in the other decreases for a given direction of applied acceleration. Thus,

$$f_{r,1} = B_1 \sqrt{F_I + F_S}$$

$$f_{r,2} = B_2 \sqrt{F_I - F_S}$$

where

$f_{r,1}$ resonant frequency of ribbon attached to m_1

$f_{r,2}$ resonant frequency of ribbon attached to m_2

B_1, B_2 constants

As shown in figure 6, each ribbon is made flat and placed in a magnetic field in such an orientation that electric current passed through it will cause deflection perpendicular to the field. Each ribbon-magnet system is used as the tuning element in an oscillator circuit whose output is a sinusoidal signal with frequency a function of acceleration. The signals from the two oscillators are mixed and filtered to pass just the difference frequency given by

$$f_{r,1} - f_{r,2} = B_1 \sqrt{F_I + F_S} - B_2 \sqrt{F_I - F_S} \quad (1)$$

Careful control during manufacture yields

$$B_1 = B_2 = B$$

So that application of the binomial expansion to equation (1) gives

$$f = f_{r,1} - f_{r,2} = B \left(F_I^{1/2} + \frac{1}{2} F_I^{-1/2} F_S - \frac{1}{8} F_I^{-3/2} F_S^2 + \frac{1}{16} F_I^{-5/2} F_S^3 - \dots + \dots \right. \\ \left. - F_I^{1/2} + \frac{1}{2} F_I^{-1/2} F_S + \frac{1}{8} F_I^{-3/2} F_S^2 + \frac{1}{16} F_I^{-5/2} F_S^3 + \dots + \dots \right) \\ f = B F_I^{-1/2} \left(F_S + \frac{1}{8} \frac{F_S^3}{F_I^2} - \dots + \dots \right)$$

With $F_I \gg F_S$ for the design span of the instrument

$$f \cong B \frac{F_S}{\sqrt{F_I}} \quad (2)$$

or the output frequency is directly proportional to the force caused by acceleration.

Electrical system. - One of the restraints on the electrical system, imposed by the payload design, was that standard IRIG FM/FM telemetry was to be used. If an accelerometer had been selected whose output was a dc voltage level proportional to acceleration, then this signal would have been used as the input to a standard IRIG voltage-controlled oscillator. Since the very slight rate of change of this signal would have been swamped by the drift of a voltage-controlled oscillator, this method was impractical (see the sec-

tion Accelerometer Analysis, p. 16). This is precisely the reason for the selection of the particular type of accelerometer that was used. Its output, a sinusoidal voltage whose frequency was proportional to acceleration, was well suited to the telemetry since its output looked like a subcarrier channel.

The basic quantity to be measured was the time rate of change of this frequency, which, as will be shown, was directly proportional to thrust. It will be shown in the section Accelerometer Analysis (eq. (25), p. 19) that this frequency-time function was modulated by a sinusoidal term whose amplitude was proportional to $\tan \theta$, where θ is the precession half-cone angle. The overall or long term frequency-time function was then a ramp, whose slope was proportional to thrust, with a sinusoidal modulation whose

amplitude was proportional to $\tan \theta$ (see fig. 7).

The electrical system was required to perform three functions:

- (1) Accurately measure the slope of the frequency-time function ramp
- (2) Measure the amplitude and frequency of the modulation

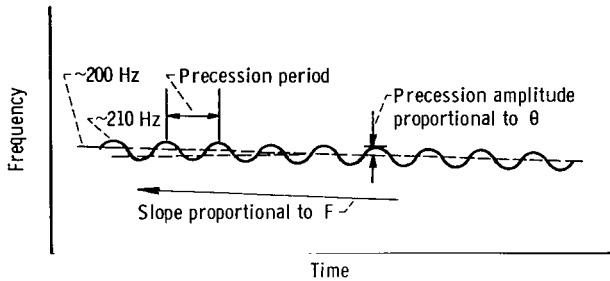


Figure 7. - General form of accelerometer output (not to scale).

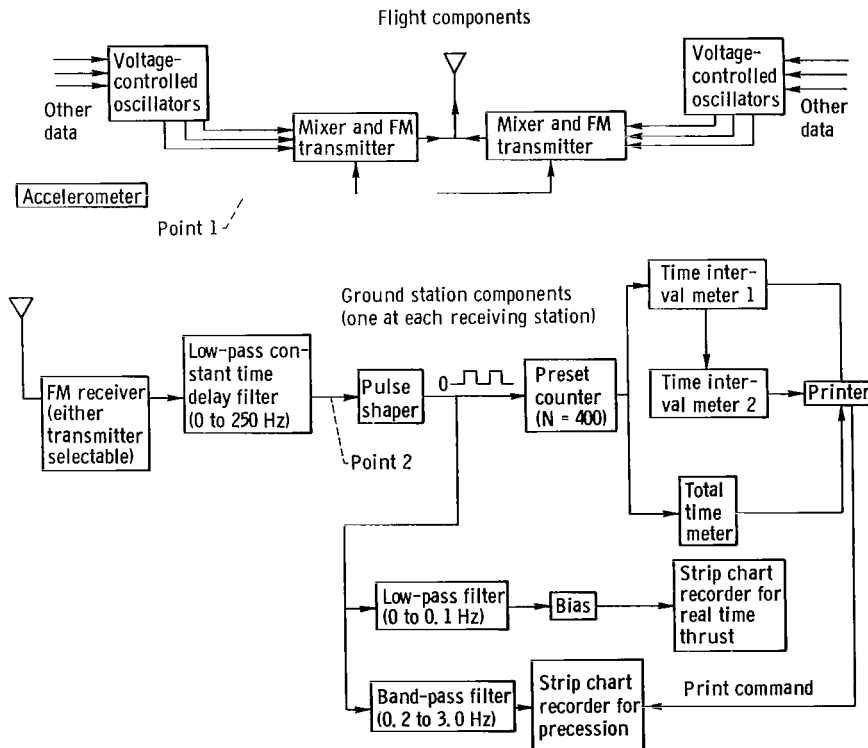


Figure 8. - Accelerometer electrical system.

(3) Provide a real time indication of thrust

A block diagram of the electrical system is shown in figure 8.

The accelerometer signal was mixed with the standard subcarrier outputs and used to modulate the transmitter. On the ground, the received signal was demodulated and passed through a constant time delay filter to separate the accelerometer signal from the other data channels. The sinusoidal accelerometer signal at point 1 was then reproduced at point 2.

This signal was applied to a pulse shaper whose output was a short rise time pulse occurring at the time of each positive-going zero crossing of the input. This pulse was one of constant amplitude and width, so that the time average value of the pulse train voltage was directly proportional to frequency.

Accurate digital measurement of ramp slope: An accurate measure of the ramp slope was achieved by using a preset counter to put out 1 pulse for every 400 that were put in so that the time-interval meters could digitally measure the total period of time (in μsec) required for 400 cycles of the accelerometer signal to occur. Since the expected frequency was about 200 hertz, this yielded an average of the frequency over approximately 2 seconds. The two time interval meters were used in alternation in order to avoid the loss of every other 400-cycle interval.

These time interval data were then printed along with total time from the total time meter. The time rate of change of period could then be obtained from these data and, when corrected for precession effects, if necessary, thrust could be calculated.

Precession measurement: A plot of the modulation on the frequency-time signal was obtained by sending the output of the pulse shaper through a band-pass filter (0.2 to 3 Hz) and thence to a strip chart recorder. Both modulation amplitude and frequency could be obtained from this. In addition, each time the time-interval meters completed a reading, a time synchronizing pulse was sent to another channel on this same recorder so that the digital data could be corrected for the effects of precession. This would be necessary, if there were appreciable precession, because the time-interval meter sampling times would not always correspond to equivalent levels on the modulation, or, in other words, aliasing would be introduced.

Real time thrust indication: It was also required that an indication of thrust be available during flight. This was accomplished by passing the pulse train through a low-pass filter (0 to 0.1 Hz), the output of which was applied to a dc bias voltage in series with a high-sensitivity strip chart recorder. During the flight the slope of this record, and hence the thrust, was read with a protractor.

ANALYSIS

The basic goal of the thrust detection system was to measure the thrust to an accuracy of about ± 5 percent with as short an averaging time as possible (10 to 60 sec) so that a plot of thrust against time could be obtained with reasonable thrust and time resolution. Since the thrust of the contact ion thruster was expected to be 7.1 millinewtons, whereas that of the bombardment ion thruster was expected to be 25 millinewtons, the detection system, if sufficiently accurate to measure the contact ion thruster thrust level, would certainly be sufficiently accurate for the bombardment ion thruster. Thus, the analysis will be based on the thrust level of the contact ion thruster.

Sun Sensor Analysis

Spin detection. - The equation for thrust in terms of sun sensor period measurements is obtained from the general equation for a rotating body

$$F x_t = \frac{d}{dt} (I \omega_z) = \frac{dI}{dt} \omega_z + I \frac{d\omega_z}{dt} \quad (3)$$

With the worst case spacecraft temperature rise assumed, the term containing the rate of change of mass moment of inertia was calculated to be less than 0.4 percent of the contact ion thruster thrust and is, therefore, considered negligible. The equation may be rewritten, with F assumed constant over an interval Δt ,

$$F x_t = I \frac{\Delta \omega_z}{\Delta t} \quad (4)$$

Since

$$\omega_z = \frac{2\pi}{P} \quad (5)$$

and

$$\omega_z, M = \frac{2\pi}{P_M}$$

where M is an integer,

$$F x_t = I \frac{2\pi(P_M - P_1)}{P_1 P_M \Delta t} \quad (6)$$

where $P_1 \simeq P_M = P$ because of the very low torque to inertia ratio, and Δt may be defined as MP , where M is the number of periods between measurements.

The thrust may then be written as

$$F = \frac{2\pi I}{x_t} \frac{\Delta P}{MP^3} \quad (7)$$

Equation (7) assumes the following:

- (1) No external torques other than the engine are acting on the spacecraft.
- (2) The rate of change of inertia due to thermal expansion of the spacecraft is negligible.
- (3) The engine is thrusting normal to its moment arm and normal to the spin axis. (See the section on accelerometer errors, p. 21, for consideration of this effect.)
- (4) The spin rate ω_z is pure spin about the z-axis (i. e., no precession or nutation).
- (5) The thrust is constant over the measurement interval.

Errors. - The errors in thrust measurement by the sun sensor system may be thought of as mechanical and electrical, and most of them are derivable from equation (7). The effects of precession (assumption (4)) are not derivable from equation (7) and will be treated separately.

Mechanical: The error in thrust due to mass moment of inertia uncertainties is given by

$$\left(\frac{dF}{F}\right)_I = \frac{dI}{I} \leq 1 \text{ percent}$$

The uncertainty of the effective thrust vector location with respect to the spacecraft center of gravity gives rise to an error in F of

$$\left(\frac{dF}{F}\right)_{x_t} = \frac{dx_t}{x_t} \leq 1 \text{ percent}$$

These two mechanical errors would be relatively constant through the flight and should contribute a probable error of about 1 percent.

Electrical: The electrical errors are the errors of the sun sensor system itself.

They are the errors associated with sensing, transmitting, receiving, and measuring the spacecraft period.

The error in thrust due to the error in measuring period is given by

$$\left(\frac{dF}{F}\right)_P = \frac{2 dP}{\Delta P} - \frac{3 dP}{P} \quad (8)$$

and since $\Delta P \ll P$

$$\left(\frac{dF}{F}\right)_P \approx \frac{2 dP}{\Delta P} \quad (9)$$

Evaluation of equation (9) requires calculation of the expected values of P and ΔP . For the contact ion thruster, ΔP may be computed from equation (7) to be

$$\Delta P = \frac{FMP^3 x_t}{2\pi I} \quad (10)$$

Then with the parameters listed in table I

TABLE I. - PARAMETERS

Parameter	Design value	Actual value
Mass moment of inertia about x-axis, I_x	-----	10.0 (kg)(m ²)
Mass moment of inertia about y-axis, I_y	-----	11.3 (kg)(m ²)
Mass moment of inertia about z-axis, I_z	14.4 (kg)(m ²)	14.3 (kg)(m ²)
k	0.3	-----
Thruster moment arm, x_t	0.557 m	0.557 m
Sun sensor period, P	0.628 sec	0.7048 sec
Initial angular velocity about z-axis, ω_z	10 rad/sec	8.97 rad/sec
Initial half-cone angle, θ	3.5×10^{-2} rad (2°)	5.3×10^{-4} rad (0.03°)
Thrust of contact ion thruster, F_c	7.1 mN	-----
Thrust of bombardment ion thruster, F_b	25 mN	22 mN
Accelerometer location, R'	0.262 m	0.262 m
Accelerometer scale factor, K	$7.83 (H_z)(\text{sec}^2)/\text{m}$	$7.83 (H_z)(\text{sec}^2)/\text{m}$
Cycles of accelerometer signal, N	400	400

$$\Delta P = 10M (\mu\text{sec}) \quad (11)$$

The variation between successive period measurements dP was determined experimentally. A pulsed light source was used to energize the sun sensor at a rate of 2 pulses per second. The voltage pulse that fired the light was connected to the start input of the time interval meter system. The stop input was energized by way of light pulse, sun sensor, telemetry link, and discriminator output. Essentially, the time delay of the sun sensor system (a few msec) was being measured. Data were taken over periods of minutes with the spacecraft in the vacuum chamber with and without ion engines thrusting. Plots of the data for any given run show a maximum spread in the time delay of ± 25 microseconds. However, close analysis of the data showed that the majority of successive readings differed by only about ± 5 microseconds, and a much lower frequency drift was causing the wider spread in data.

When a worst case, dP of ± 5 microseconds, is assumed, the error in thrust is given from equation (9) to be

$$\left(\frac{dF}{F}\right)_P = \frac{2 \times 5}{10M} = \frac{1}{M} \quad (12)$$

which says that the thrust must integrate over 10 periods or 6.3 seconds to reduce the error to ± 0.7 millinewton or 10 percent of the full-scale thrust.

Precession: The assumption that the spacecraft is not precessing or nutating leads to two possible errors. The first would be an apparent scatter in the period measurement introduced by precession. This scatter should be periodic with time and, therefore, removable from the data. The second arises from the fact that, if the spacecraft is coning initially, and if the cone angle damps out during the thrust measurement, then the energy contained in the precession mode may couple into the spin axis and cause an apparent thrust.

An analysis of this second source of error begins by assuming cylindrical symmetry so that the kinetic energy of rotation is

$$KE = \frac{1}{2} I \omega_z^2 + \frac{1}{2} I_N (\omega_x^2 + \omega_y^2) \quad (13)$$

If all of the energy in the precession mode would couple into the spin mode and there were no dissipation, then, for

$$\theta_1 = \text{initial cone angle}$$

$$\theta_2 = \text{final cone angle}$$

and

$$J_z = J \cos \theta \quad (14)$$

the kinetic energy would be

$$KE_1 = \frac{1}{2} I \omega_{z,1}^2 \left(1 + \frac{I}{I_N} \tan^2 \theta_1 \right) \quad (15)$$

$$KE_2 = \frac{1}{2} I \omega_{z,2}^2 \left(1 + \frac{I}{I_N} \tan^2 \theta_2 \right) \quad (16)$$

With $\theta_2 = 0$ equations (15) and (16) reduce to

$$\omega_{z,1}^2 \frac{I}{I_N} \tan^2 \theta_1 = \omega_{z,2}^2 - \omega_{z,1}^2 \quad (17)$$

Simplifying and assuming $\omega_{z,1} \cong \omega_{z,2}$ and $\tan \theta_1 = \theta_1 = 0.035$ radian give

$$\Delta \omega_z \cong \frac{\omega_z}{2} \frac{I}{I_N} \theta_1^2 \quad (18)$$

$$= \frac{10}{2} (1.34)(0.035)^2$$

$$= 83 \times 10^{-4} \text{ rad/sec} \quad (19)$$

If the coupling took place uniformly over 500 seconds (about one-half the expected operating time of each thruster), the angular acceleration would be

$$\frac{\Delta \omega_z}{\Delta t} = 1.7 \times 10^{-5} \text{ rad/sec}^2$$

as compared with $\dot{\omega}_z \simeq 2.5 \times 10^{-4}$ radian per second² for the contact ion thruster and 8.8×10^{-4} radian per second² for the bombardment ion thruster. The error in F would be

$$\left(\frac{dF}{F}\right)_\theta \cong \frac{1.7 \times 10^{-5}}{2.5 \times 10^{-4}} \cong 7 \text{ percent} \quad (20)$$

for the contact ion thruster or 2 percent for the bombardment ion thruster.

TABLE II. - SUMMARY OF CALCULATED ERRORS
IN SUN SENSOR SYSTEM

Source	Error	
	In thrust of contact ion thruster, F_c	In thrust of bombardment ion thruster, F_b
Mass moment of inertia about z-axis, I_z	< 1 percent	< 1 percent
Thruster moment arm, x_t	< 1 percent	< 1 percent
Sun sensor period, P^a	± 7 mN	± 2 mN
Half-cone angle, θ^b	7 percent	2 percent
Ultimate error with long averages	1 percent	1 percent

^a $dP = \pm 5 \mu\text{sec}$; $M = 10$.

^bDamping from 0.035 rad to 0 in 500 sec.

Summary: The error in thrust measurement for the sun sensor system depended chiefly on the scatter of the period measurement and the possible coupling of energy from precession to spin (table II). If the scatter were considerably less than the measured ± 5 microseconds or if longer averages could be taken, this source of error would be reduced. If the rate of precession energy transfer were considerably less than the assumed value, this error would be reduced. The minimum error expected was that contributed by the mechanical parameters or ± 1 percent. Even with no energy-transfer effects and period-measurement scatter, this ± 1 percent error would be present.

Accelerometer Analysis

An additional thrust detection system was incorporated both as a backup for the sun sensor system and as a means of precession detection. The single-axis accelerometer described previously was selected to provide these functions.

Location and orientation. - The accelerometer was located at point R (fig. 1, p. 3) with position vector \vec{R} . With the accelerometer at R it was necessary to determine the optimum orientation of the sensitive axis with respect to \vec{R} and the optimum location of R. The first case considered was $y_a = R$ and $x_a = z_a \cong 0$ with the sensitive axis perpendicular to \vec{R} and parallel to the x, y-plane. In this case, the accelerometer would have been used to sense $R\dot{\omega}_z$, which is a direct measure of thrust ($F = I\dot{\omega}_z/x_t$). However, this orientation is impractical because of the tolerance on alinement of the sensitive axis and of the thrust axis. There would be a cross-axis centripetal acceleration on

the accelerometer equal to $R\omega_z^2$. Even if the instrument had zero cross-axis sensitivity, a misalignment of the sensitive axis from perpendicularity to \vec{R} of only 5 microradians (1 arc sec) would result in a component of this centripetal acceleration along the sensitive axis equal to $5 \times 10^{-6} R\omega_z^2$. Taking the ratio between this undesired component and the desired $R\dot{\omega}_z$ component gives $5 \times 10^{-6} \omega_z^2 / \dot{\omega}_z$. Since $\omega_z \simeq 10$ radians per second and $\dot{\omega}_z \simeq 2.5 \times 10^{-4}$ radians per second² for the contact ion thruster, this ratio is 2, which means that the undesired component would be about twice as large as the desired component. This is the result even under the most optimistic assumptions of zero cross-axis sensitivity and axis alignment to within 5 microradians.

The alternative was to measure $R\omega_z^2$, the centripetal component, directly and from this detect the rate of change which would be proportional to thrust. The requirements in this case were for an extremely stable instrument since it was to detect accurately a very small change in a very large quantity. Taking the ratio of the change in acceleration to the acceleration for an averaging time Δt of 10 seconds shows this clearly:

$$\begin{aligned} \frac{2R\omega_z \dot{\omega}_z \Delta t}{R\omega_z^2} &= \frac{2\dot{\omega}_z \Delta t}{\omega_z} \\ &= \frac{2 \times 2.5 \times 10^{-4} \times 10}{10} = 5.0 \times 10^{-4} \\ &= 0.05 \text{ percent} \end{aligned}$$

Thus, the quantity of interest is only about 0.05 percent of the quantity being measured directly. Since the requirement was for 5 percent accuracy on thrust, the required accuracy in the measurement of a change in acceleration was $0.05 \times 5 \times 10^{-4} = 2.5 \times 10^{-5} = 0.0025$ percent. The accelerometer used for this was described in the section Accelerometer (p. 7). It was sufficiently stable to meet these stringent requirements.

Once it had been established that the measurement of $\dot{\omega}_z$ by means of detecting the rate of change of centripetal acceleration was feasible, it remained to determine the optimum orientation of the sensitive axis with respect to \vec{R} because \vec{R} might not lie in the x, y-plane. The sensitive axis could be oriented either parallel to \vec{R} or perpendicular to the z-axis. The orientation chosen should be that which would enable more direct measurement of the centripetal acceleration and produce the more readily interpretable function of thrust.

Consider the case where the sensitive axis is parallel to \vec{R} . The radial acceleration at R would be

$$a_{\mathbf{R}} = \frac{\ddot{\vec{\mathbf{R}}} \cdot \vec{\mathbf{R}}}{R} \quad (21)$$

$$\ddot{\vec{\mathbf{R}}} = \dot{\vec{\omega}} \times \vec{\mathbf{R}} + \vec{\omega} \times (\vec{\omega} \times \vec{\mathbf{R}}) \quad (22)$$

$$a_{\mathbf{R}} = \frac{\dot{\vec{\omega}} \cdot (\vec{\mathbf{R}} \times \vec{\mathbf{R}})}{R} + \frac{[\vec{\omega}(\vec{\mathbf{R}} \cdot \vec{\omega}) - \vec{\mathbf{R}}(\vec{\omega} \cdot \vec{\omega})] \cdot \vec{\mathbf{R}}}{R} \quad (23)$$

$$a_{\mathbf{R}} = -R\omega^2 \sin^2 \angle(\vec{\omega}, \vec{\mathbf{R}}) \quad (24)$$

The significant feature of this result is that $a_{\mathbf{R}}$ would depend only on ω , and not on $\dot{\omega}$. This fact is important in that it would make the accelerometer signal more readily interpretable. The time rate of change of $a_{\mathbf{R}}$ would be directly proportional to thrust for small change in ω and not complicated by dependence on $\ddot{\omega}$.

If the sensitive axis were aligned other than along $\vec{\mathbf{R}}$, an equation for the acceleration along the sensitive axis, similar to equation (22), would result. However, the term proportional to $\dot{\vec{\omega}}$ would not be zero because there would be no $\vec{\mathbf{R}} \times \vec{\mathbf{R}}$ multiplier as in equation (22). The measured acceleration would be a function of $\dot{\vec{\omega}}$, and the time derivative of this acceleration would be a function of $\ddot{\vec{\omega}}$. Thus, the interpretation of this acceleration function in terms of thrust would be more complex. This analysis led to the orientation of the accelerometer parallel to $\vec{\mathbf{R}}$. As can be seen from equation (23), the ideal location of $\vec{\mathbf{R}}$ would have been in the x,y-plane since this would maximize $\sin \angle(\vec{\omega}, \vec{\mathbf{R}})$. However, physical restraints of the payload prevented this exact location; that is, there was insufficient room on the plane so that the accelerometer had to be mounted under the disk.

Acceleration as function of time. - With the accelerometer located at R and oriented parallel to $\vec{\mathbf{R}}$, the acceleration $a_{\mathbf{R}}$ as a function of time along that vector at that point had to be determined.

The basic equations used to determine $a_{\mathbf{R}}$ are Euler's dynamical equations

$$L_x = I_x \dot{\omega}_x + (I_z - I_y) \omega_z \omega_y$$

$$L_y = I_y \dot{\omega}_y - (I_z - I_x) \omega_z \omega_x$$

$$L_z = I_z \dot{\omega}_z + (I_y - I_x) \omega_x \omega_y$$

The solution to these three equations for $a_{\mathbf{R}}$ as a function of time was obtained on a

digital computer. However, because of the complexity, a few simplifying assumptions will be made at this point to yield an analytically obtainable and interpretable solution. Features of this solution that differ significantly from the computer solution will be made evident in the section RESULTS.

The simplifying assumptions are

(1) $I_x = I_y$ (cylindrical symmetry).

(2) $\dot{\omega}_z = 0$. Even though $\dot{\omega}_z$ was the basic quantity to be measured, ω_z was a very slowly varying function of time because of the small torque of the ion thruster and will be considered constant over a few precession periods.

(3) $L_x = L_y = 0$. This is really not an assumption if perfect alinement of the ion thrusters is assumed and there are no extraneous torques.

Appendix C shows the derivation of a_R , the result of which is

$$a_R = R\omega_z^2 \left[\cos^2 \beta - \frac{I \tan \theta \sin 2\beta}{I_N} \cos(k\omega_z t - \delta) \right] \quad (25)$$

Equation (25) can now be written in the form

$$a_R = R'\omega_z^2 [1 - C_1 \cos(k\omega_z t - \delta)] \quad (26)$$

where

$$C_1 = 2 \frac{I}{I_N} \tan \theta \tan \beta \approx 0.046 \quad (27)$$

$$k = \frac{I}{I_N} - 1 \quad (28)$$

$$R' = R \cos^2 \beta \quad (29)$$

which is seen to be a steady acceleration with a ripple term whose amplitude is approximately 5 percent of the steady state (see eq. (27)). The presence of the angle δ is seen to do nothing more than shift the phase of the ripple as seen by the accelerometer.

Thrust measurement. - In the last section it was shown that

$$a_R = R'\omega_z^2 \quad (30)$$

if the small ripple term is neglected. In actuality this term could not be neglected, but an analysis based on its being zero was used and the result was corrected for the ripple.

The instrument used was a single-axis accelerometer whose output was a sinusoidal electrical signal whose frequency was a direct, linear function of acceleration (see eq. (2)):

$$f = Ka_R \quad (31)$$

Deviations from this response were shown to be negligible in the section Accelerometer (p. 7).

The equation relating this frequency to thrust can then be obtained:

$$F = \frac{I\alpha}{x_t} \quad (32)$$

where $\alpha = \dot{\omega}_z$

$$f = KR'\omega_z^2$$

$$\dot{f} = 2KR'\omega_z\alpha \quad (33)$$

$$F = \frac{I\dot{f}}{2x_tKR'\omega_z} \quad (34)$$

$$F = \frac{I\dot{f}}{2x_t\sqrt{KR'f}} \quad (35)$$

With

$$K = 7.83 \frac{(\text{Hz})(\text{sec}^2)}{\text{m}} \quad (36)$$

$$R' = 0.262 \text{ m} \quad (37)$$

the initial frequency would be

$$f_0 \approx 205 \text{ Hz} \quad (38)$$

With

$$F_c = 7.1 \text{ mN} \quad (39)$$

$$I = 14.4(\text{kg})(\text{m}^2) \quad (40)$$

$$x_t = 0.557 \text{ m} \quad (41)$$

the angular acceleration resulting from full-scale contact ion thruster thrust would be

$$\alpha_c = 2.75 \times 10^{-4} \text{ rad/sec}^2 \quad (42)$$

so that for a 10-second interval ($\Delta t = 10$)

$$\frac{\dot{f} \Delta t}{f} = \frac{2\alpha \Delta t}{\dot{\omega}_z} = 5.5 \times 10^{-4} \quad (43)$$

The accuracy requirement, or 5 percent of this, is about 0.0028 percent. Thus, it has been shown that the accuracy required for measurement of f was 0.0028 percent for 10-second averaging time to 0.015 percent for 60-second averaging time.

Errors. - The errors in thrust measurement by the accelerometer system can be divided into two categories, mechanical and electrical.

Mechanical: In order to take into account the inaccuracies of the locations of the accelerometer and thruster, equation (35) can be rewritten

$$F = \frac{\dot{f}}{2x_t \sin \angle(\vec{F}, \vec{x}_t) \sqrt{KfR' \cos \angle(\vec{A}, \vec{R}')}} \quad (44)$$

where \vec{A} is the sensitive axis of the accelerometer. Then

$$\left(\frac{dF}{F}\right)_m = \frac{dI}{I} - \frac{dx_t}{x_t} - \frac{d \angle(\vec{F}, \vec{x}_t)}{\tan \angle(\vec{F}, \vec{x}_t)} - \frac{1}{2} \frac{dR'}{R'} + \frac{1}{2} \left[\tan \angle(\vec{A}, \vec{R}') \right] d \angle(\vec{A}, \vec{R}') \quad (45)$$

It was determined by prelaunch measurements that

$$\frac{dI}{I} \approx \frac{dx_t}{x_t} \approx \frac{dR'}{R'} \leq 0.01 \quad (46)$$

For small misalignments the remaining two terms involving angular misalignment can be rewritten

$$\frac{d \angle(\vec{F}, \vec{x}_t)}{\tan \angle(\vec{F}, \vec{x}_t)} = \tan \left[\frac{\pi}{2} - \angle(\vec{F}, \vec{x}_t) \right] d \angle(\vec{F}, \vec{x}_t) \quad (47)$$

$$\frac{d \angle(\vec{F}, \vec{x}_t)}{\tan \angle(\vec{F}, \vec{x}_t)} \simeq \left[\frac{\pi}{2} - \angle(\vec{F}, \vec{x}_t) \right]^2 \quad (48)$$

$$\frac{1}{2} \left[\tan \angle(\vec{A}, \vec{R}') \right] d \angle(\vec{A}, \vec{R}') = \frac{1}{2} \left[\angle(\vec{A}, \vec{R}') \right]^2 \quad (49)$$

These terms would contribute only 0.5 and 0.25 percent, respectively, for misalignments of 0.07 radian. The actual alignment was assumed to be within this limit for the thrust vector and was known to be within 0.02 radian for the accelerometer.

In summary, then, the probable error due to mechanical measurement inaccuracies was less than 2 percent.

Electrical: The terms in equation (44) that were ignored in the previous section are

$$\left(\frac{dF}{F} \right)_e = \frac{\dot{f}}{f} - \frac{1}{2} \frac{df}{f} - \frac{1}{2} \frac{dK}{K} \quad (50)$$

Their size can be determined as follows.

(1) Accelerometer scale factor K . The effect on F of an uncertainty in K is really twofold, the term shown and the effect on f of a rate of change in K , \dot{K} . The latter will be examined first:

$$f = KR' \omega_z^2 \quad (51)$$

$$\dot{f} = 2KR' \omega_z \alpha + R' \omega_z^2 \dot{K} \quad (52)$$

It will be shown that the second term in equation (52) is negligible (less than 1 percent) compared with the first; therefore, the effect of \dot{K} can be neglected. The maximum allowable value for \dot{K} can be obtained by taking the ratio of the two terms:

$$\frac{R' \omega_z^2 \dot{K}}{2KR' \omega_z \alpha} = \frac{\omega_z \dot{K}}{2K\alpha} < 0.01 \quad (53)$$

$$\frac{\dot{K}}{K} < 0.01 \frac{2\alpha}{\omega_z} \approx \frac{10^{-2} \times 2 \times 2.75 \times 10^{-4}}{10} \quad (54)$$

$$\frac{\dot{K}}{K} < 5.5 \times 10^{-7} \text{ sec}^{-1} \quad (55)$$

This was true for the accelerometer used and furthermore was the primary reason for the choice of such a high quality accelerometer. Since the accelerometer was of such quality, the effect of an uncertainty in K could be neglected.

(2) Time interval meter count uncertainty dT . The remaining error in electrical measurement was then traceable to the measurement of f :

$$\left(\frac{dF}{F}\right)_e = \frac{df}{f} - \frac{1}{2} \frac{df}{f} \quad (56)$$

Now

$$\dot{f} = \frac{f_2 - f_1}{\Delta t} \quad (57)$$

Thus

$$\frac{\dot{df}}{\dot{f}} = \frac{d(f_2 - f_1)}{f_2 - f_1} - \frac{d \Delta t}{\Delta t} \quad (58)$$

Since the measurements of f_2 and f_1 are separate but subject to the same errors,

$$\frac{\dot{df}}{\dot{f}} = \frac{2 df}{\Delta f} - \frac{d \Delta t}{\Delta t} \quad (59)$$

Since Δt was of the order of 2 seconds and $d \Delta t$ of the order of 10^{-6} second, the $d \Delta t / \Delta t$ term could easily be neglected:

$$\left(\frac{dF}{F}\right)_e = df \left(\frac{2}{\Delta f} - \frac{1}{2f}\right) \quad (60)$$

However, $\Delta f \ll f$, and thus

$$\left(\frac{dF}{F}\right)_e = \frac{2 df}{\Delta f} \quad (61)$$

Since the time interval meters did not actually measure f but T , the period of N cycles of f ($N = 400$), it is necessary to express equation (61) in terms of T and dT :

$$f = \frac{N}{T} \quad (62)$$

$$df = -\frac{N}{T^2} dT = -\frac{f dT}{T} \quad (63)$$

$$\Delta f = \dot{f} \Delta t \quad (64)$$

$$\Delta f = 2KR' \omega_z \alpha \Delta t \quad (65)$$

$$\Delta f = \frac{2f \alpha \Delta t}{\omega_z} \quad (66)$$

$$\frac{2 df}{\Delta f} = -\frac{\omega_z N dT}{f \alpha \Delta t T^2} \quad (67)$$

Since the data were being taken continuously,

$$\Delta t = T \quad (68)$$

$$\frac{2 df}{\Delta f} = -\frac{\omega_z N dT}{f \alpha T^3} \quad (69)$$

$$\frac{2 df}{\Delta f} = -\frac{\omega_z f^2}{\alpha N^2} dT \quad (70)$$

Equation (70) brings to light the need for the preset counter since it can be seen that a fairly large N is required to bring this error to the level of about 1 percent. Neverthe-

less N must be kept as small as possible to allow time resolution of thrust.

When values are applied to equation (70),

$$\frac{2 \, df}{\Delta f} \approx - \frac{10}{2.75 \times 10^{-4}} \frac{200^2}{400^2} \times 10^{-6} \quad (71)$$

$$\frac{2 \, df}{\Delta f} \approx 0.01 \text{ or } 1 \text{ percent} \quad (72)$$

where dT was taken as the 1 count (1 μ sec) uncertainty of the time interval meters.

(3) Electrical noise. In this section the required signal-to-noise ratio of the signal input to the pulse shaper will be established on the basis of a maximum dT of 1 microsecond. In the previous section dT was taken as the 1 count uncertainty of the digital counters. This would be the error limit if the signal input to the pulse shaper were perfectly noise free.

If the signal is assumed to be a pure sine wave (of frequency f) with additive noise, then it can be readily shown that the following relation exists among the voltage signal-to-noise ratio S/\mathcal{N} , the error in time of the pulse shaper trigger τ , and the frequency f :

$$\frac{S}{\mathcal{N}} = \frac{1}{\pi f \tau} \quad (73)$$

With $f \approx 200$

$$\tau = 10^{-6} \text{ (the resolution of the counters)}$$

$$\frac{S}{\mathcal{N}} = 16 \times 10^2 \text{ or } 64 \text{ db} \quad (74)$$

Equation (74) shows that the required signal-to-noise ratio was about 64 decibels.

(4) Variation in filter time delay $d\tau_f$. It will be shown in this section that the time delay of the low-pass filter (see fig. 8, p.9) had to be constant (within a tolerance) over the frequency range of interest.

If the time of the first positive zero crossing of the signal at the input to the filter is taken as zero, the result is a positive zero crossing at the output at

$$t_1 = \tau_{f,1} \quad (75)$$

where $\tau_{f,1}$ is the time delay of the filter at frequency f_1 .

The N^{th} positive-going zero crossing emerges from the filter N cycles later at time

$$t_2 = T + \tau_{f,2} \quad (76)$$

$$\tau_{f,2} = \tau_{f,1} + \frac{\partial \tau_f}{\partial f} \Delta f \quad (77)$$

$$t_2 - t_1 = T + \frac{\partial \tau_f}{\partial f} \Delta f \quad (78)$$

From equations (65), (68), and (78)

$$t_2 - t_1 = T \left(1 + 2KR' \omega_z \alpha \frac{\partial \tau_f}{\partial f} \right) \quad (79)$$

In order that $t_2 - t_1$ be considered equal to T within 1 microsecond,

TABLE III. - SUMMARY OF CALCULATED ERRORS
IN ACCELEROMETER SYSTEM

Source	Error	
	In thrust of contact ion thruster, F_c , percent	In thrust of bombardment ion thruster, F_b , percent
Mass moment of inertia about z-axis, I_z	< 1	< 1
Thruster moment arm, x_t	< 1	< 1
Accelerometer location, R'	< 1	< 1
Thruster alinement, $\angle(\vec{F}, \vec{x}_t)$	< .5	< .5
Accelerometer alinement $\angle(\vec{A}, R')$	< .25	< .25
Accelerometer scale factor, K , and \dot{K}	< 1	< 1
Frequency of accelerometer signal, f , or period of N accelerometer signal cycles, T^a	< 1	< 1
Ultimate error expected	< 5	1

^aFor $dT = \pm 1 \mu\text{sec}$; $N = 400$; $S/N = 64 \text{ db}$.

$$\frac{d\tau_f}{df} < 45 \mu\text{sec/Hz} \quad (80)$$

The filter was a special design which met this requirement.

Summary: The total probable error in thrust measurement for the accelerometer system was expected to be 3 to 5 percent of the thrust of the contact ion thruster (table III).

RESULTS

The SERT I spacecraft was launched July 20, 1964, in a ballistic trajectory. The contact ion thruster failed to start because of a high-voltage breakdown. The bombardment ion thruster operated for a total of about 30 minutes, during which time it was stopped and successfully restarted a number of times (ref. 1). While operating it produced a measured thrust of about 22 millinewtons.

The fact that only the larger of the thrusters operated made the task of thrust detection less critical than would have been the case if the smaller thruster had functioned. The following sections will discuss the results obtained from the thrust detection systems.

Sun Sensor Data

Figure 9 is a plot of spin period against time as determined by the sun sensor shortly after arm deployment. These data are typical of those obtained during periods of zero thrust throughout the flight. During periods of thrust the average value of period sloped markedly upward. The sun sensor period oscillated about its average value of 0.70480 second at 0.47 hertz or one-third the spin frequency with a peak-to-peak deviation of approximately 300 microseconds. This modulation at one-third the spin frequency was caused by precession and remained throughout the flight, while the peak-to-peak

deviation decreased almost linearly to about 100 microseconds at the end of the flight.

Because the period data were modulated at one-third the spin frequency, the thrust was computed by letting M equal 3 in the thrust equation (eq. (7)). The difference between successive third periods

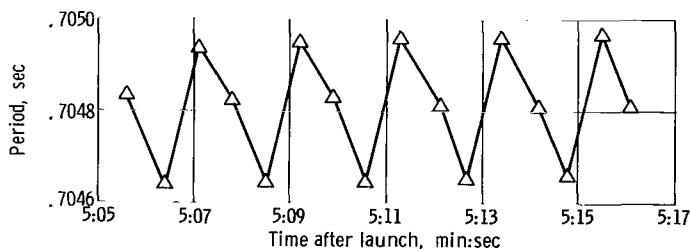


Figure 9. - Sun sensor period as function of time. Data taken from Wallops Island ground station.

showed a jitter of about 5 microseconds, in agreement with that observed during pre-flight ground testing. This gives an error due to jitter of ± 1.7 millinewtons or ± 8 percent of full-scale bombardment ion thruster thrust over a measurement time of only 2 seconds. Because the contact ion thruster failed to work, the spacecraft coasted for several minutes. The spin rate during coast was observed to be constant within the observable limits, which verified the assumption of negligible external torque and indicated that there was negligible energy coupling into the spin axis.

The sun sensor data provided an average thrust measurement over 2 seconds to within about ± 9 percent of full-scale thrust. When the thrust was constant for 30 seconds or more, the error was determined primarily by the mechanical tolerances on the spacecraft. Thus, these longer averages approached an accuracy of ± 1 percent.

Accelerometer Data

Precession. - In the analysis it was assumed that the payload was cylindrically symmetrical. In practice this was not the case since the actual mass moments of inertia were

$$I_x = 10.0 \text{ (kg)(m}^2\text{)}$$

$$I_y = 11.3 \text{ (kg)(m}^2\text{)}$$

$$I_z = 14.3 \text{ (kg)(m}^2\text{)}$$

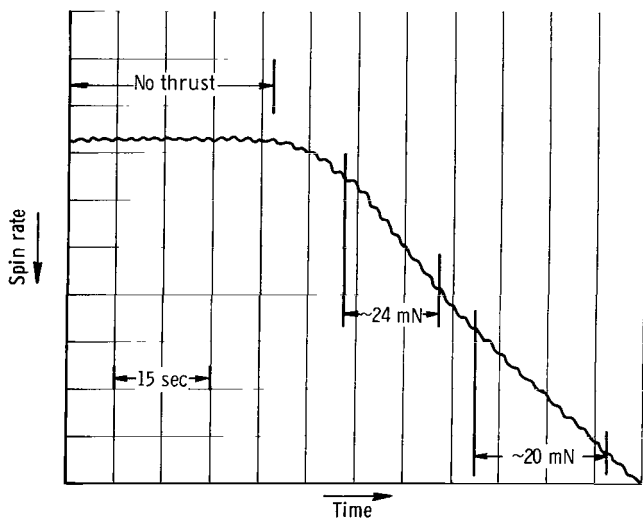


Figure 10. - Real time thrust record.

The principal effect of this lack of symmetry on the accelerometer analysis was to make invalid the result that θ was a constant in time. In other words, nutation was introduced. Because of the complexity that nutation introduces into the analysis, a digital computer solution of Euler's equations was used in conjunction with the data from the strip chart record of precession to determine the actual value of θ and its variation with time. (See the section on the accelerometer electrical system, p. 8.) During the first portion

of flight ($\omega_z = 8.97$ rad/sec) θ oscillated between 3.5×10^{-4} (0.02°) and 5.3×10^{-4} radian (0.03°) and gradually decayed to about one-third of this value in agreement with sun sensor data. The value of θ calculated from equation (25) for the first portion of the flight was 7.4×10^{-4} radian (0.042°), which indicates that the assumption of symmetry was warranted. The gradual decay of θ indicated that energy from the precession mode may have been coupling to the spin mode at a fairly constant rate. However, the small value of θ indicated negligible initial energy in the precession mode compared with the energy change of the spin mode due to thrust. Thus, correction for the precession energy transfer effect on the thrust data was not necessary.

The period of the modulation of accelerometer frequency output, as determined from the same strip chart record and in agreement with the computer solution, was about 2.1 seconds as compared with 2.05 seconds calculated from equation (25).

Thrust (real time readout). - Thrust readout was accomplished in real time as described in the section on the accelerometer electrical system (p. 8). A section of the strip chart record is reproduced in figure 10. The horizontal axis is time, and the vertical axis is spin rate, though it should be noted that the vertical axis on this plot represents only a small portion of the total spin rate since most of the signal was electrically biased out. The slope of the plot is proportional to thrust. It can be seen from this plot that the 22-millinewton thrust was detected with ample resolution for real time readout. The small oscillation on this record represents that portion of the precession-caused modulation that the low-pass filter failed to exclude. Its period is 2.1 seconds, as explained in the previous section.

Thrust (digital readout). - Thrust was calculated as a function of time from the digital data recorded from the time-interval meters. Because of the very small cone angles that were measured, the digital data were used without correction for precession energy transfer. Each value of the time interval required for 400 cycles of accelerometer output frequency was subtracted from the previous value. From this difference was calculated \dot{f} for the mean point in time. Equation (35) was then used to calculate F.

The major problem encountered with these thrust data was the fact that, during certain portions of the flight, the sampling period (i. e., the period of 400 cycles) was just a bit longer than the period of precession. This led to large aliasing error. Figure 11 (p. 30) shows a plot of thrust against time for the period T + 27 minutes to T + 28 minutes, a period chosen to illustrate the large effects of aliasing. From figure 11 it can be seen that the uncorrected accelerometer data, averaged over a minute, agree with the sun sensor data. A point-by-point correction for this aliasing, obtained by applying equation (25) to the data from the strip chart record of precession, yielded corrected accelerometer data (also shown in fig. 11) which agreed very well with the sun-sensor data.

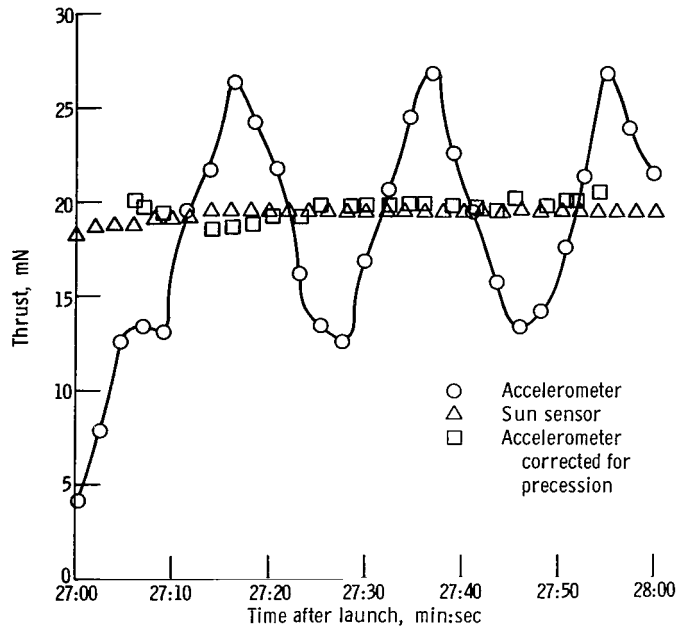


Figure 11. - Accelerometer and sun sensor thrust data with large aliasing effect.

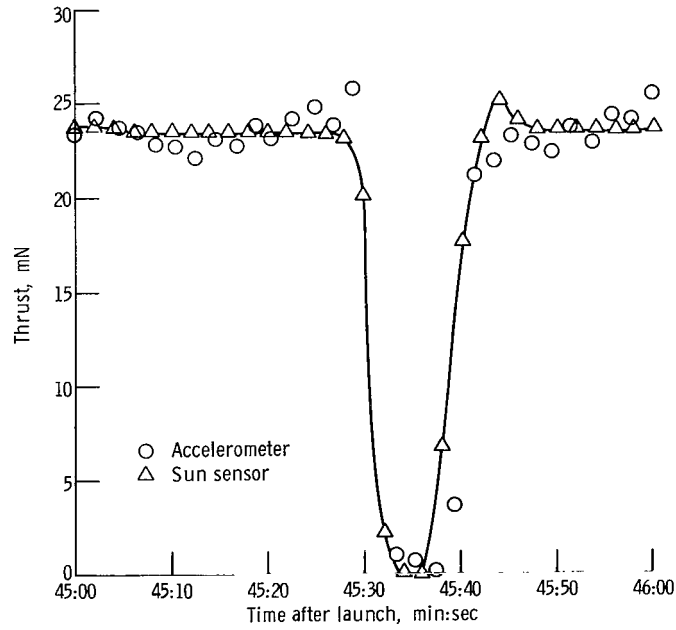


Figure 12. - Accelerometer and sun sensor thrust data with negligible aliasing effect.

Figure 12 shows a plot of thrust against time for the period $T + 45$ minutes to $T + 46$ minutes, a period chosen to illustrate the results obtained when negligible aliasing was observed. It can be seen that the accelerometer data and sun-sensor data agree during this period even through a short period of engine shutdown. The accelerometer data were not corrected for aliasing in figure 12.

CONCLUDING REMARKS

From the data presented in the preceding sections it is seen that the thrust of the bombardment ion thruster was measured with agreement to within 5 percent between the sun-sensor and accelerometer thrust detection systems. That the two systems complemented each other is evident from the fact that the accelerometer data showed the precession angle to be sufficiently small so that the sun-sensor data could be treated as being relatively free from the energy transfer effect. The sun-sensor data were used, on the other hand, to make an in-flight check of the accelerometer operation during the period of no thrust.

It should be pointed out, in conclusion, that the use of a radial accelerometer, as on this payload, provided a very sensitive means of detecting small precession angles. This was shown by both the simplified analysis and the results.

Lewis Research Center,
National Aeronautics and Space Administration,
Cleveland, Ohio, January 5, 1966.

APPENDIX A

SYMBOLS

A	sensitive axis of accelerometer	I	maximum principal mass moment of inertia
$\angle(\vec{A}, \vec{R})$	angle between vectors \vec{A} and \vec{R}	I_N	principal mass moment of inertia normal to I (assuming cylindrical symmetry)
a	acceleration	I_x, I_y, I_z	mass moments of inertia about x, y, and z, respectively
a_R	acceleration along R	i, j, k	unit vectors along x, y, and z, respectively
B_1, B_2	constants	J	angular momentum
F	thrust	J_z	angular momentum about z-axis
$\left(\frac{dF}{F}\right)_I$	error in F due to errors in I (typical notation used throughout)	K	accelerometer scale factor
F_b	thrust of bombardment ion thruster	KE	kinetic energy
F_c	thrust of constant ion thruster	k	$\frac{I}{I_N} - 1$
F_I	initial tension in accelerometer spring	L_x, L_y, L_z	torque about x, y, and z, respectively
F_S	force on "proof mass" of accelerometer due to acceleration	M	number of periods of sun sensor data
f	frequency of accelerometer signal	m	mass
f_r	resonant frequency of accelerometer string	N	number of cycles of accelerometer signal
f_0	initial frequency of accelerometer signal	P	sun sensor period or time of one spacecraft revolution
		R	location of accelerometer or magnitude of \vec{R}

R'	$R \cos^2 \beta$	τ	time-interval meter resolution
S/\mathcal{N}	signal-to-noise ratio	τ_f	filter time delay at frequency f
T	period of N accelerometer signal cycles	ω	angular velocity
t	time	$\omega_x, \omega_y, \omega_z$	angular velocities about x , y , and z , respectively
x, y, z	principal axes of spacecraft (see fig. 1)	$\omega_{x,0}$	ω_x at $t = 0$
x_a, y_a, z_a	location of accelerometer (see fig. 1)	Subscripts:	
x_t	location of either ion thruster	e	electrical
α	angular acceleration	M	M th period
α_c	angular acceleration due to contact ion thruster thrust	m	mechanical
β	defined by fig. 1	Superscripts:	
δ	defined by fig. 1	$(\vec{\quad})$	vector
θ	half-cone angle (see fig. 1)	$(\dot{\quad}), (\ddot{\quad})$	first and second time derivatives
σ	standard deviation		

APPENDIX B

METHOD OF COMPUTING ANGLE BETWEEN A CELESTIAL BODY AND SPIN AXIS OF A SPIN STABILIZED SPACECRAFT

The SERT I spacecraft has two sun sensor systems mounted on the periphery of the spacecraft baseplate. As the spacecraft spins about its axis of maximum moment of inertia, the sun sensor views or "sweeps out" a triangle of revolution, as shown in figure 13. The limits of the triangle of revolution are determined by the geometry of the sun sensor housing and may be expressed as angles measured from the spin axis. To ensure illumination of the sensor by the sun and to prevent illumination by the Earth and the moon, the angle between the spacecraft spin axis and the sun must be controlled. The trajectory of the SERT I spacecraft and, hence, the attitude of the spin axis was optimized for maximum experiment time. The launch window is then the time interval during which the angle between the spin axis and the sun is within the limits of the triangle of revolution swept out by the sun sensor.

A general solution of the angle between the spin axis of a spin-stabilized spacecraft and the sun or any other celestial body can be calculated as a function of Greenwich mean time.

The following basic assumptions are made:

- (1) The spacecraft coordinates are fixed and known with respect to an inertial reference system at rocket burnout and are constant because of spin stabilization.
- (2) The angle between the spin axis and the sun is constant throughout the flight, because of the relatively small distance traveled in the ballistic trajectory compared to the distance from the sun.

The solution is obtained by projecting the position of the sun, the spacecraft center of gravity, and the spacecraft spin axis on to the celestial sphere (as shown in figure 14) and solving for the angle between the spin axis and the sun with spherical trigonometry.

The sun may be located on the celestial sphere by finding the Greenwich hour angle or longitude and the declination or latitude as a function of Greenwich mean time in The American Ephemeris and Nautical Almanac (ref. 4). The spacecraft center of gravity may be located by knowing its longitude and latitude at

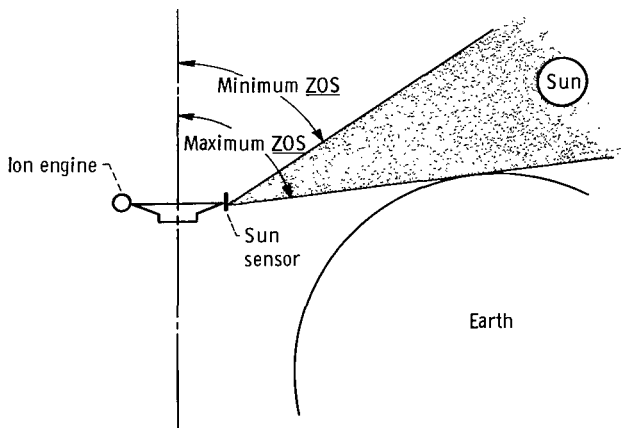


Figure 13. - Sun sensor orientation with respect to sun and Earth.

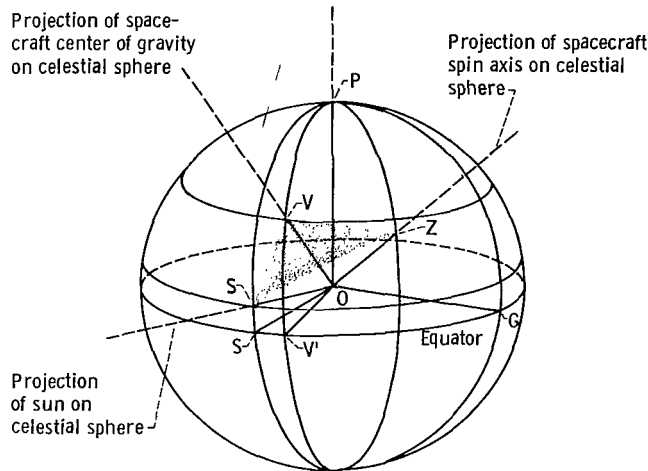


Figure 14. - Celestial sphere.

booster engine burnout. Finally, the spin axis is located by knowing the pitch and azimuth at booster engine burnout. From figure 14, the following angles are defined:

- PVS calculated
- PVZ azimuth of spin axis
- SOP colatitude of sun
- SVZ calculated
- VOP colatitude of spacecraft center of gravity
- VOS angle between local vertical and sun
- VOZ copitch of spin axis
- VPS local hour angle
- ZOS angle between spin axis and sun

From the law of cosines

$$\cos \underline{VOS} = \cos \underline{SOP} \cos \underline{VOP} + \sin \underline{SOP} \sin \underline{VOP} \cos \underline{VPS} \quad (\text{B1})$$

From the law of sines

$$\sin \underline{PVS} = \frac{\sin \underline{SOP} \sin \underline{VPS}}{\sin \underline{VOS}} \quad (\text{B2})$$

$$\underline{SVZ} = 360^{\circ} - \underline{PVZ} - \underline{PVS}$$

From the law of cosines

$$\cos \underline{ZOS} = \cos \underline{VOS} \cos \underline{VOZ} + \sin \underline{VOS} \sin \underline{VOZ} \cos \underline{SVZ} \quad (B3)$$

A digital computer was used to solve the preceding equations in 1-hour increments. Figure 15 shows the angle between the spin axis of the SERT I spacecraft and the sun (angle \underline{ZOS}) plotted as a function of Greenwich mean time for July 20, 1964. The shaded portions indicate the maximum and minimum limits of the triangle of revolution swept out by the sun sensor. The intersection of these limit lines and angle \underline{ZOS} define the time limits of the flight. It is apparent that there are two launch windows, one in the morning and one in the afternoon. When the angle between the spin axis and the moon is plotted, however, the moon is seen to cross through the afternoon window.

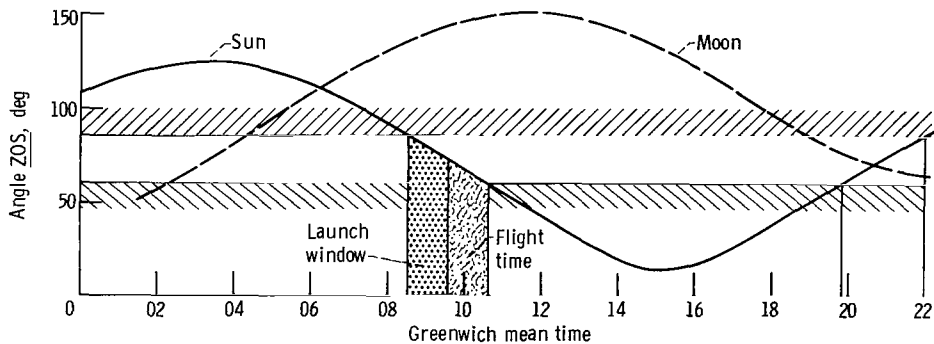


Figure 15. - Angle between SERT I spin axis and sun and spin axis and moon as function of Greenwich mean time for July 20, 1964.

APPENDIX C

DERIVATION OF MEASURED ACCELERATION AS FUNCTION OF TIME

The derivation of a_R as a function of time is accomplished by starting with Euler's dynamical equations

$$L_x = I_x \dot{\omega}_x + (I_z - I_y) \omega_z \omega_y$$

$$L_y = I_y \dot{\omega}_y - (I_z - I_x) \omega_z \omega_x$$

$$L_z = I_z \dot{\omega}_z + (I_y - I_x) \omega_x \omega_y$$

and the assumptions explained in the text

$$I_x = I_y$$

$$\dot{\omega}_z = 0$$

$$L_x = L_y = 0$$

If these assumptions are applied and

$$I_z = I \tag{C1}$$

$$I_x = I_y = I_N \tag{C2}$$

$$k = \frac{I - I_N}{I_N} \tag{C3}$$

the result is

$$\dot{\omega}_x + k \omega_y \omega_z = 0 \tag{C4}$$

$$\dot{\omega}_y - k \omega_x \omega_z = 0 \tag{C5}$$

Equations (C4) and (C5) are two simultaneous linear differential equations with constant coefficients. With the choice of $\omega_y = 0$ at $t = 0$ the solutions are

$$\omega_x = \omega_{x,0} \cos k\omega_z t \quad (C6)$$

$$\omega_y = \omega_{x,0} \sin k\omega_z t \quad (C7)$$

It is necessary to express a_R in terms of ω_y and ω_x . From equations (21) and (22)

$$\begin{aligned} a_R &= \frac{[\vec{\omega} \times (\vec{\omega} \times \vec{R})] \cdot \vec{R}}{R} \\ a_R &= \frac{(\vec{R} \times \vec{\omega}) \cdot (\vec{\omega} \times \vec{R})}{R} \\ a_R &= -\frac{(\vec{R} \times \vec{\omega})^2}{R} \end{aligned} \quad (C8)$$

Neglecting the negative sign (which merely indicates that a_R is centripetal) and expanding yield

$$\begin{aligned} a_R &= \frac{1}{R} \left[\vec{i}(y_a \omega_z - z_a \omega_y) + \vec{j}(z_a \omega_x - x_a \omega_z) + \vec{k}(x_a \omega_y - y_a \omega_x) \right]^2 \\ a_R &= \frac{1}{R} \left[x_a^2 (\omega_y^2 + \omega_z^2) + y_a^2 (\omega_x^2 + \omega_z^2) + z_a^2 (\omega_x^2 + \omega_y^2) - 2(y_a z_a \omega_y \omega_z + x_a z_a \omega_x \omega_z + x_a y_a \omega_x \omega_y) \right] \end{aligned} \quad (C9)$$

From figure 1

$$x_a = -R \cos \beta \cos \delta \quad (C10)$$

$$y_a = -R \cos \beta \sin \delta \quad (C11)$$

$$z_a = -R \sin \beta \quad (C12)$$

Substituting equations (C10), (C11), and (C12) into equation (C9) gives

$$\begin{aligned} a_R &= R \left[\cos^2 \beta \cos^2 \delta (\omega_y^2 + \omega_z^2) + \cos^2 \beta \sin^2 \delta (\omega_x^2 + \omega_z^2) \right. \\ &\quad \left. + \sin^2 \beta (\omega_x^2 + \omega_y^2) - 2(\cos \beta \sin \beta \sin \delta \omega_y \omega_z \right. \\ &\quad \left. + \cos \beta \sin \beta \cos \delta \omega_x \omega_z + \cos^2 \beta \sin \delta \cos \delta \omega_x \omega_y) \right] \end{aligned} \quad (C13)$$

These expressions, for ω_y and ω_x and for a_R in terms of ω_y , ω_x , and ω_z , must be combined with an expression for θ in terms of $\omega_{x,0}$, which can be obtained by considering the invariance of the angular momentum vector:

$$J_z = J \cos \theta \quad (C14)$$

$$I\omega_z = \sqrt{I^2\omega_z^2 + I_N^2(\omega_x^2 + \omega_y^2)} \cos \theta \quad (C15)$$

$$\tan \theta = \frac{I_N \sqrt{\omega_x^2 + \omega_y^2}}{I\omega_z} \quad (C16)$$

From equations (C6), (C7), and (C16) or from figure 1,

$$\tan \theta = \frac{I_N \omega_{x,0}}{I\omega_z} \quad (C17)$$

Thus

$$\omega_{x,0} = \frac{I}{I_N} \omega_z \tan \theta \quad (C18)$$

and

$$\begin{aligned} a_R = R\omega_z^2 & \left\{ \cos^2 \beta \cos^2 \delta \left[1 + \left(\frac{I \tan \theta}{I_N} \right)^2 \sin^2 k\omega_z t \right] \right. \\ & + \cos^2 \beta \sin^2 \delta \left[1 + \left(\frac{I \tan \theta}{I_N} \right)^2 \cos^2 k\omega_z t \right] + \sin^2 \beta \left(\frac{I}{I_N} \tan \theta \right)^2 \\ & - 2 \frac{I \tan \theta}{I_N} \left(\cos \beta \sin \beta \sin \delta \sin k\omega_z t + \cos \beta \sin \beta \cos \delta \cos k\omega_z t \right. \\ & \left. \left. + \frac{I \tan \theta}{I_N} \cos^2 \beta \sin \delta \cos \delta \sin k\omega_z t \cos k\omega_z t \right) \right\} \quad (C19) \end{aligned}$$

After trigonometric simplification

$$a_R = R\omega_z^2 \left\{ \cos^2 \beta + \frac{1}{2} \left(\frac{I \tan \theta}{I_N} \right)^2 \left[1 + \sin^2 \beta - \cos^2 \beta \cos 2(k\omega_z t - \delta) \right] - \frac{I \tan \theta}{I_N} \sin 2\beta \cos(k\omega_z t - \delta) \right\} \quad (C20)$$

The first term gives the expected acceleration if θ were zero; the second is a quantity oscillating at frequency $k\omega_z/\pi$ and amplitude $1/2 \left[(I/I_N) \tan \theta \cos \beta \right]^2 R\omega_z^2$; the third is a quantity oscillating at one-half the frequency of the second and amplitude $R\omega_z^2 (I/I_N) \tan \theta \sin 2\beta$.

In order to interpret this equation, it is necessary to look at some of the relative magnitudes that result when the following numerical values are assumed:

$$\beta = 0.473 \text{ radian - actual value}$$

$$\delta = 0.84 \text{ radian - actual value}$$

$$\theta = 0.035 \text{ radian - maximum allowed by dampers}$$

$$R = 0.33 \text{ m - actual value}$$

$$\omega_z = 10 \text{ rad/sec - assumed initial value}$$

$$\frac{I}{I_N} = 1.3 \text{ - approximate average of } \frac{I_z}{I_x} \text{ and } \frac{I_z}{I_y}$$

The ratio of the amplitude of the third term to that of the second (in eq. (C20)) yields

$$\frac{2 \sin 2\beta}{\frac{I}{I_N} \tan \theta \cos^2 \beta} = \frac{4 \tan \beta}{\frac{I}{I_N} \tan \theta} \simeq 45 \quad (C21)$$

so that the second term amounts to nothing more than a small amount of second harmonic distortion on the third term.

Equation (C20) reduces to the following if the second term is neglected:

$$a_R = R\omega_z^2 \left[\cos^2 \beta - \frac{I \tan \theta \sin 2\beta}{I_N} \cos(k\omega_z t - \delta) \right] \quad (C22)$$

REFERENCES

1. Cybulski, Ronald J. ; Shellhammer, Daniel M. ; Lovell, Robert R. ; Domino, Edward J. ; and Kotnik, Joseph T. : Results From SERT I Ion Rocket Flight Test. NASA TN D-2718, 1965.
2. Gold, Harold; Rulis, Raymond J. ; Maruna, Frank A. , Jr. ; and Hawersaat, William H. : Description and Operation of Spacecraft in SERT I Ion Thrustor Flight Test, NASA TM X-52050, 1964.
3. Kerslake, William R. ; and Pawlik, Eugene V. : Additional Studies of Screen and Accelerator Grids for Electron-Bombardment Ion Thrustors. NASA TN D-1411, 1963.
4. Anon: The American Ephemeris and Nautical Almanac. U.S. Government Printing Office, 1964.

"The aeronautical and space activities of the United States shall be conducted so as to contribute . . . to the expansion of human knowledge of phenomena in the atmosphere and space. The Administration shall provide for the widest practicable and appropriate dissemination of information concerning its activities and the results thereof."

—NATIONAL AERONAUTICS AND SPACE ACT OF 1958

NASA SCIENTIFIC AND TECHNICAL PUBLICATIONS

TECHNICAL REPORTS: Scientific and technical information considered important, complete, and a lasting contribution to existing knowledge.

TECHNICAL NOTES: Information less broad in scope but nevertheless of importance as a contribution to existing knowledge.

TECHNICAL MEMORANDUMS: Information receiving limited distribution because of preliminary data, security classification, or other reasons.

CONTRACTOR REPORTS: Technical information generated in connection with a NASA contract or grant and released under NASA auspices.

TECHNICAL TRANSLATIONS: Information published in a foreign language considered to merit NASA distribution in English.

TECHNICAL REPRINTS: Information derived from NASA activities and initially published in the form of journal articles.

SPECIAL PUBLICATIONS: Information derived from or of value to NASA activities but not necessarily reporting the results of individual NASA-programmed scientific efforts. Publications include conference proceedings, monographs, data compilations, handbooks, sourcebooks, and special bibliographies.

Details on the availability of these publications may be obtained from:

SCIENTIFIC AND TECHNICAL INFORMATION DIVISION
NATIONAL AERONAUTICS AND SPACE ADMINISTRATION
Washington, D.C. 20546